Mechanistic inferences of the photocatalyzed oxidation of chlorinated phenoxyacetic acids by electrospray mass spectral techniques and from calculated point charges and electron densities on all atoms

Natsuko Watanabe,[a] Satoshi Horikoshi,[a] Kouji Suzuki,[a] Hisao Hidaka*[a] and Nick Serpone*[b]

[a] *Frontier Research Center for the Global Environment Protection (EPFC), Meisei University, 2-1-1 Hodokubo, Hino, Tokyo 191-8506,, Japan. E-mail: hidaka@epfc.meisei-u.ac.jp*
[b] *Department of Chemistry and Biochemistry, Concordia University, 1455 de Maisonneuve Blvd. West, Montreal, PQ H3G-1M8,, Canada. E-mail: serpone@vax2.concordia.ca*

Received* (*in Montpellier, France*) *2nd December 2002, Accepted 6th January 2003
First published as an Advance Article on the web 8th April 2003

The photodegradation of 2,4-dichlorophenoxyacetic acid (2,4-D) taking place in UV irradiated aqueous TiO_2 dispersions was revisited to obtain mechanistic details on the basis of similar degradation of the related 2,3-dichlorophenoxyacetic acid (2,3-D), 4-chlorophenoxyacetic acid (4-M) and phenoxyacetic acid (PhA). Mechanistic changes were inferred from the different positions of the chlorine substituents. As well, the compounds were compared for differences in degradation rate and initial adsorption on the TiO_2 surface as a function of the number of chlorines. The initial mechanistic sequence(s) in the TiO_2-photocatalyzed oxidation of each substrate was predicted theoretically by molecular orbital (MO) calculations of frontier electron densities and point charges of all the atoms in the phenoxyacetic acid structures.

Introduction

The agrochemical 2,4-dichlorophenoxyacetic acid (2,4-D) is a popular product in agriculture used extensively worldwide as a herbicide. However, 2,4-D is found scattered in various natural ecosystems with potentially serious consequences to human organisms.[1] This herbicide is a highly toxic material listed by the Japanese Ministry of the Environment and by the U.S. Environmental Protection Agency as a suspected endocrine disruptor. Accordingly, the degradation of 2,4-D necessitates immediate disposal, since chlorine-containing compounds are typically difficult to biodegrade naturally.

Photocatalytic decomposition of pollutants on TiO_2 semiconductor particles in aqueous media has been shown to be an effective and attractive oxidation method in the general area of Advanced Oxidation Technologies. Several chlorinated compounds have been degraded photocatalytically by UV illuminated TiO_2, for example 2,4-D,[2–4] dibromochloropropane,[5–7] hexachlorocyclohexane,[7] and *p*,*p*'-DDT.[8,9]

This article focuses on a comparison of the photodegradation process of four phenoxyacetic acids differing in the number ($n = 0$, 1, 2) and/or position of the chlorine substituents, as exemplified by 2,4-dichlorophenoxyacetic acid, 2,3-dichlorophenoxyacetic acid (2,3-D), 4-chlorophenoxyacetic acid (4-M), and phenoxyacetic acid (PhA), to extract mechanistic details of the photodegradation of the 2,4-D herbicide.

Experimental

Materials

Reagent grade 2,4-dichlorophenoxyacetic acid, 2,3-dichlorophenoxyacetic acid, 4-chlorophenoxyacetic acid, and phenoxyacetic acid were supplied by Wako Pure Chem. Co. Ltd (see structures below; all atoms are labelled with a number for the MO calculations). The photocatalyst was Degussa P-25 titanium dioxide (TiO_2) whose particle size was 20–30 nm (determined from transmission electron microscopy); its surface area was 53 m^2g^{-1} (BET methods) and the crystalline structure was 83% anatase and 17% rutile as determined by X-ray diffraction analysis.

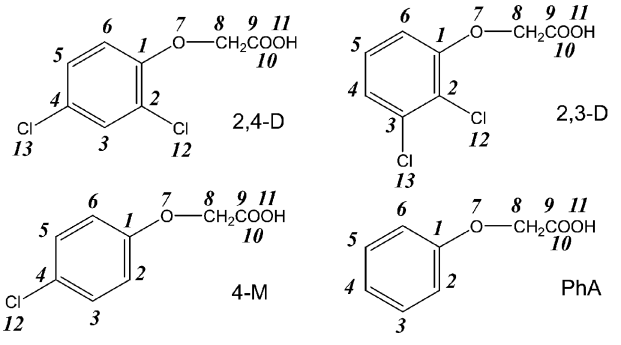

Photodegradation procedures and analytical methods

Aqueous solutions (0.1 mM, 50 mL) of the four acids were placed in a 124 mL Pyrex vessel containing TiO_2 particles (loading, 100 mg). The resulting dispersion was subsequently purged with oxygen gas and then supersonicated. Irradiation of the dispersions was carried out with a 75 W Hg lamp emitting an irradiance of *ca.* 2.0 mW cm^{-2} in the wavelength range 310 to 400 nm (maximal emission at $\lambda = 360$ nm).

Ring-opening of the benzene moiety (*i.e.*, loss of aromaticity) was analyzed with a JASCO V-560 UV/VIS spectrophotometer. The concentration of chloride ions was assayed with a JASCO liquid chromatograph (HPLC) equipped with a CD-5 conductivity detector and an anion column (I-524). The temporal evolution of CO_2 was monitored by gas chromatography with a Shimadzu GC-8AIT (TCD detection) using a Porapack Q column; helium was the carrier gas. The temporal decrease of total organic carbon (TOC) was determined with a Shimadzu TOC-5000A analyzer. Formation of carboxylic acid

 DOI: 10.1039/b211963n

intermediates during the photooxidation of the various specimens was followed with a JASCO liquid chromatograph (HPLC) containing bromothymol blue (BTB); the column was a KC-811 and the UV detector was set at 445 nm. The intermediates were identified by direct injection into the mass spectral detector of an Agilent Technologies 1100 LC-MSD (electrospray ionization: API-ESI) system operated in the negative mode; the capillary voltage was 2800 V. The eluent was a solution of acetonitrile–H_2O (1:1). Note that the LC column was not used in this study. The flow rate of the sheath of heated dry nitrogen gas (heater temperature, 300 °C) was maintained at 10 L min^{-1} and the gas pressure was 40 psi. The spectrometer was scanned from m/z 50 to 300 at 0.3 mL min^{-1} during the recording of mass spectra. The injected 10 μL volume of a sample solution was loaded using an Agilent Technologies 1100 auto-sampling device.

Computer simulations

Computer simulations and relevant MO calculations were carried out with a CAChe Worksystem version 3.2 (Fujitsu Co. Ltd) implemented on an Intel P-IV/Windows XP system personal computer to obtain frontier electron densities (to infer points of radical attack) and point charges of all the atoms in the phenoxyacetic acids (see above structures). The geometrical configuration was determined by pre-optimization calculations using the Mechanics software with augmented MM3, followed by geometrically optimized calculations in MOPAC using AM1 parameters. Solvation effects of water were simulated by the COSMO method.[10–12]

Results and discussion

Past experience has shown that TiO_2 particles absorb UV light of energy greater than the bandgap (*ca.* 3.2 eV for anatase and 3.0 eV for rutile) to generate electron/hole pairs [eqn. (1)]. Following various steps, the holes (h^+) are ultimately trapped by HO^- ions (or H_2O) at the particle surface to yield $^{\bullet}OH$ radicals [and H^+; eqn. (2)]. Our data do not preclude the possibility of direct hole scavenging by the 2,4-D to form cation radicals; however under our conditions, this scenario was rather unlikely. Concomitantly, dioxygen molecules react with conduction band electrons (e^-) to yield superoxide radical anions, $O_2^{-\bullet}$, which on protonation generate the hydroperoxy, $^{\bullet}OOH$, radicals [eqns. (3a) and (3b)].

$$TiO_2 + h\nu \rightarrow TiO_2\ (e^- + h^+) \rightarrow e^- + h^+ \quad (1)$$

$$h^+ + OH^-_{surf}\ (\text{and/or } H_2O) \rightarrow {}^{\bullet}OH + H^+ \quad (2)$$

$$e^-_{cb} + O_2 \rightarrow O_2^{-\bullet} \quad (3a)$$

$$O_2^{-\bullet} + H^+ \rightarrow {}^{\bullet}OOH \quad (3b)$$

$$^{\bullet}OH\ (\text{or } {}^{\bullet}OOH) + 2,4\text{-D} \rightarrow \text{Oxidative products} \quad (4)$$

The TiO_2 particle surface is positively charged (pH less than 6.3) owing to excess protons produced in reaction 2, or because the solution is initially acidic (*ca.* pH = 3.5–3.7), changing a Ti–OH neutral surface to a $Ti–OH_2^+$ positive surface. Accordingly, negatively charged atoms in the 2,4-D structure will be attracted on the surface of TiO_2 by simple Coulombic forces. Moreover, the $^{\bullet}OH$ radicals photogenerated on the TiO_2 surface are expected to be the major oxidative agents to attack the substrates adsorbed on the surface through the most negatively charged atoms of the phenoxyacetic acids.

The characteristics of the photodegradation of 2,4-D, 2,3-D, 4-M and PhA, through predicted initial steps, were examined by molecular orbital calculations (MO) of frontier electron densities and point charges on all the atoms (see above structures) of the four substrates. These are summarized in Table 1. Attack of the substrates by the highly electrophilic $^{\bullet}OH$ radicals on the surface of TiO_2 is expected to occur at the atoms bearing the highest frontier electron densities. The lifetime of the $^{\bullet}OH$ radical chemisorbed on the TiO_2 surface is a few microseconds so that its reaction with the substrates is most efficient when the substrates are also chemisorbed or physisorbed. Note that the lifetime of the DMPO–$^{\bullet}OH$ adduct is about 23 min according to ESR measurements. We expect that when the distance between a negatively charged atom bound to the particle surface and an atom possessing a high frontier electron density is relatively short the photodegradation will be relatively fast.

The atoms bearing the greatest negative charge in the 2,4-D, 2,3-D, 4-M and PhA structures were in all cases the O-*10*

Table 1 Results of radical frontier electron density and point charge calculations for the 2,4-D, 2,3-D, 4-M and PhA substrates using the MOPAC system in the CAChe package

	Point charge				Radical frontier electron density			
	2,4-D	2,3-D	4-M	PhA	2,4-D	2,3-D	4-M	PhA
C-*1*	0.091	0.104	0.072	0.058	**0.356**	0.287	**0.379**	**0.356**
C-*2*	−0.113	−0.147	−0.198	−0.211	0.313	**0.321**	0.221	0.262
C-*3*	−0.094	−0.055	−0.098	−0.115	0.191	0.293	0.229	0.242
C-*4*	−0.115	−0.157	−0.125	−0.184	**0.353**	0.291	**0.418**	**0.370**
C-*5*	−0.085	−0.092	−0.102	−0.117	0.271	0.221	0.204	0.217
C-*6*	−0.190	−0.163	−0.167	−0.182	0.181	0.273	0.238	0.287
O-*7*	−0.226	−0.237	−0.244	−0.250	0.123	0.120	0.129	0.137
C-*8*	−0.044	−0.037	−0.043	−0.042	0.004	0.007	0.005	0.007
C-*9*	0.402	0.398	0.401	0.401	0.020	0.019	0.036	0.069
O-*10*	**−0.490**	**−0.491**	**−0.492**	**−0.494**	0.007	0.007	0.013	0.024
O-*11*	**−0.339**	**−0.339**	**−0.340**	**−0.340**	0.003	0.003	0.005	0.009
Cl-*12*	0.006	0.020	−0.026	–	0.071	0.080	0.107	–
Cl-*13*	−0.012	0.004	–	–	0.093	0.061	–	–
H-*12*	–	–	–	−0.170	–	–	–	0.000
H-*13*	–	–	0.178	0.166	–	–	0.000	0.000
H-*14*	0.185	0.184	0.180	0.163	0.000	0.000	0.000	0.000
H-*15*	0.186	0.183	0.180	0.166	0.000	0.000	0.000	0.000
H-*16*	0.191	0.184	0.181	0.171	0.000	0.000	0.000	0.000
H-*17*	0.169	0.165	0.166	0.165	0.007	0.008	0.008	0.010
H-*18*	0.169	0.165	0.166	0.164	0.007	0.008	0.008	0.010
H-*19*	0.311	0.311	0.310	0.310	0.000	0.000	0.000	0.001

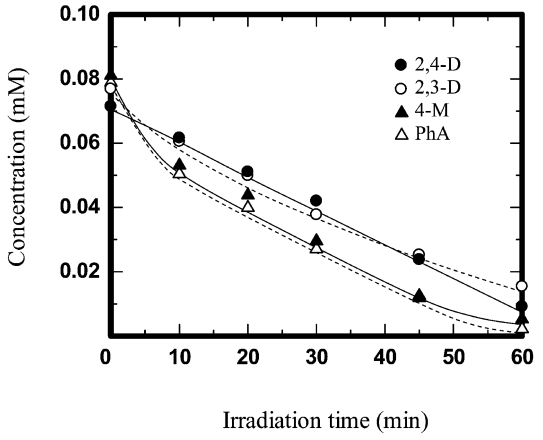

Fig. 1 Plot showing the temporal loss of the four phenoxyacetic acids as determined by UV spectral methods: 2,4-dichlorophenoxyacetic acid (2,4-D: 285 nm), 2,3-dichlorophenoxyacetic acid (2,3-D: 280 nm), 4-chlorophenoxyacetic acid (4-M: 280 nm) and phenoxyacetic acid (PhA: 268 nm) under UV illumination in air-equilibrated aqueous TiO_2 dispersions.

(−0.490 to −0.494; Table 1) followed by the O-*11* atoms (*ca.* −0.340). Therefore, each of the substrates should be no different from the others in the initial adsorption under non-irradiation conditions. Specific carbon atoms of each of the benzene rings displayed the richest frontier electron densities. They were the C-*1* and C-*4* carbons in the 2,4-D, 4-M and PhA structures, whereas only the C-*2* carbon of 2,3-D bore the largest electron density. As alluded to above, $^{\bullet}OH$ radical attack should occur predominantly on these carbon atoms. However, electron densities and point charges are not the sole factors affecting the dynamics of the photodegradation of these phenoxyacetic acids. We expect that the number and positions of the chlorine substituents will play a role on the dark adsorption/desorption equilibria and on the dynamics of the photodegradative process.

The temporal decrease of the concentration of the four phenoxyacetic acids examined, as witnessed by UV absorption losses, is illustrated in Fig. 1. Prior to UV irradiation of the various dispersions, the extent of initial adsorption of each substrate on the TiO_2 surface, estimated from initial loss of UV absorbance in the presence of titania, varied in the order 2,4-D (29%) > 2,3-D (23%) > 4-M (21%) > PhA (19%). Clearly, the initial adsorption on the TiO_2 surface appears to be proportional to the number of chlorine substituents ($n = 2,1,0$). Under UV illumination, the rate of photodegradation, as determined by UV spectroscopy, decreased in the order PhA (3.6×10^{-2} min^{-1}) > 4-M (2.6×10^{-2} min^{-1}) > 2,3-D (1.8×10^{-2} min^{-1}) > 2,4-D (1.1×10^{-2} min^{-1}); note that the latter substrate degraded *via* zero-order kinetics (1.1×10^{-3} mM min^{-1})—see Fig. 1.

Fig. 2 summarizes the dynamics of the temporal evolution of CO_2 gas and formation of Cl^- ions during the photomineralization of 2,4-D, 2,3-D, 4-M and PhA. Within experimental error, dechlorination of the three chlorinated phenoxyacetic acids occurred following identical first-order kinetics ($3.2–3.3 \times 10^{-2}$ min^{-1}). The extent of dechlorination after 180 min of irradiation was $85 \pm 5\%$. In contrast, some variation in the dynamics was observed in the formation of carbon dioxide: PhA ~ 4-M ($1.9–2.0 \times 10^{-2}$ min^{-1}) > 2,3-D ~ 2,4-D ($1.5–1.6 \times 10^{-2}$ min^{-1}). After 180 min, the mineralization yields were very similar, *ca.* $90 \pm 3\%$, for the four substrates. Evidently, the number and/or positions of the chlorine substituents influenced neither the mineralization process nor the dechlorination event. However, they did have some influence on the dark adsorption/desorption events (see above).

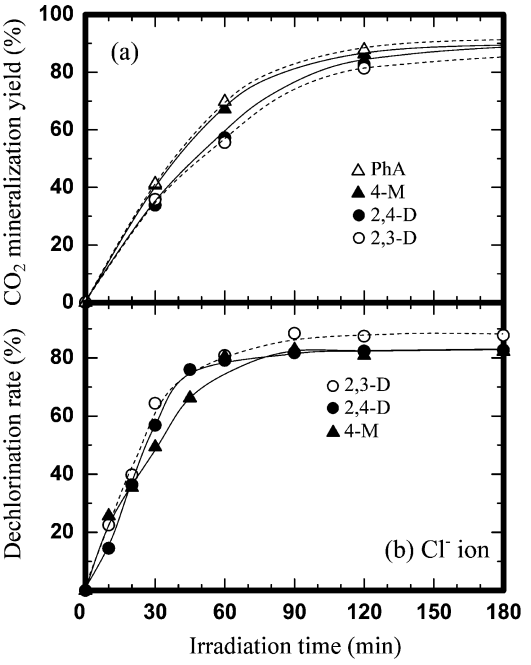

Fig. 2 Mineralization yield in CO_2 and Cl^- ions produced in the photodegradation of 2,4-D, 2,3-D, 4-M and PhA (no Cl^- ions here) in aqueous TiO_2 dispersions (100 mg in a 50 mL volume) under UV irradiation.

The temporal decrease of total organic carbon (TOC; initial concentration 9.4 ppm or 0.10 mM) during the photodecomposition of 2,4-D, 2,3-D, 4M and PhA is illustrated in Fig. 3(a). Overall, the decay of TOC followed first-order kinetics in the order (k): 2,4-D (3.2×10^{-2} min^{-1}) > PhA (2.6×10^{-2} min^{-1}) > 4-M (1.9×10^{-2} min^{-1}) > 2,3-D (1.3×10^{-2} min^{-1}). Contrary to the decrease of UV absorption and the mineralization yield as a percent of CO_2 gas evolved, the decrease of TOC for 2,4-D was more than twofold faster

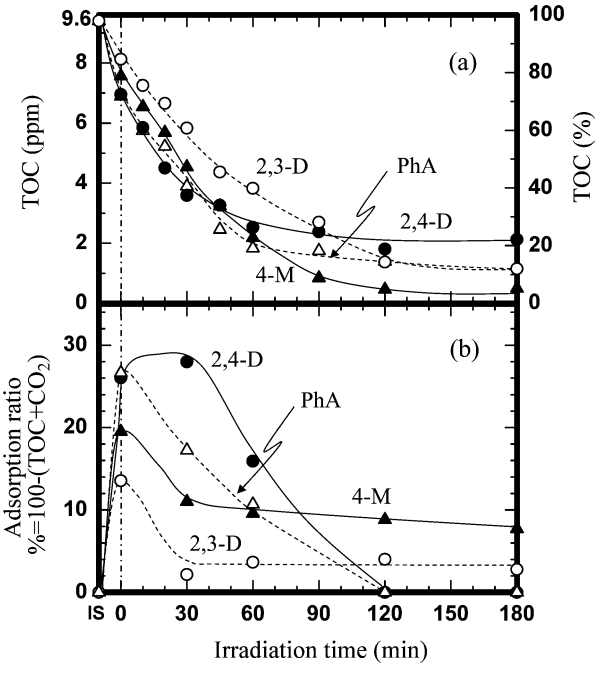

Fig. 3 (a) Temporal decrease of total organic carbon (TOC) in the photodecomposition of 2,4-D, 2,3-D, 4-M and PhA by UV illumination in aqueous TiO_2 dispersions. (b) Amount of 2,4-D, 2,3-D, 4-M and PhA and/or their respective intermediates adsorbed on the TiO_2 surface. IS denotes the initial state for the TiO_2-free solution.

than observed for 2,3-D. Two possible scenarios might explain this observation. The first is that the variation in the dynamics might reflect differences in the nature and formation of intermediates. The second possibility might be variations in the adsorption of each substrate on the TiO_2 particle surface. We discard the first because the rates of evolution of CO_2 gas are nearly identical, *viz.*, 1.5×10^{-2} min^{-1} for 2,4-D *versus* 1.6×10^{-2} min^{-1} for 2,3-D. Consequently, we look to differences in the adsorption process of the organics on the TiO_2 surface.

The extent of adsorption on the TiO_2 surface at various times was calculated from the sum of the quantity of TOC decay (in %) and the amount of CO_2 gas produced (also in %). The results are displayed in Fig. 3(b). Initially (at $t = 0$), the adsorption varied as 2,4-D ≈ PhA > 4-M > 2,3-D under dark conditions. The TOC value at zero time does not imply 100% of TOC as shown in Fig. 3(a) because of adsorption on TiO_2 surface. After an illumination period of 30 min, the order was 2,4-D > PhA > 4-M > 2,3-D. The difference in the decrease of TOC between 2,4-D and 2,3-D rests on the differences in adsorption/desorption equilibria occurring on the TiO_2 surface. We suggest that this process is affected by steric effect variations between the two substrates chemisorbed on the TiO_2 surface, as might be caused by the positions of the two chlorine atoms in the chemical structure. In the case of 2,4-D, the two adjacent molecules suffer steric repulsions between the two Cl-*12* chlorine substituents only, whereas for the 2,3-D substrate stronger steric repulsions occur between both the Cl-*12* and Cl-*13* chlorine atoms (see Scheme 1). We deduce that the gap in TOC decay behavior between the 2,4-D and 2,3-D acids is due to variations in adsorption on the TiO_2 surface and the relative positions of the chlorines. The variations in the TOC rate of decay observed for all four phenoxyacetic acids also depend on the number and positions of the chlorines in the four chemical structures.

Carboxylic acid intermediates, such as formic acid and acetic acid, were detected by HPLC techniques. Their formation and ultimate degradation to carbon dioxide are illustrated in Fig. 4(a) and 4(b), respectively. Maximal production of formic acid after only 10 min of irradiation followed nearly identical first-order kinetics for all four substrates examined; however, the quantity produced followed the order PhA (0.114 mM) > 4-M (0.102 mM) > 2,3-D (0.078 mM) > 2,4-D 0.067 mM). If the formic acid intermediate were produced from the degradation of the benzene ring, we would have expected to see a greater amount than that actually found. The increase and the decrease of the concentration of formic acid after the 10 min illumination period suggests that it was generated from the decomposition of the carboxylic acid fragment (–COOH) in the chemical structures of the phenoxyacetic acids. By contrast, formation of acetic acid was slower and the maximal quantity was observed only after irradiation for 60 min, except for 2,4-D for which it was observed after 90 min. The variation between 2,4-D and 2,3-D rests with differences in adsorption on the TiO_2 surface. We suggest that acetic acid was formed, in part, from the transformation of the acetic acid moiety ($–CH_2COOH$) and from the cleaved fragments of the benzene ring.

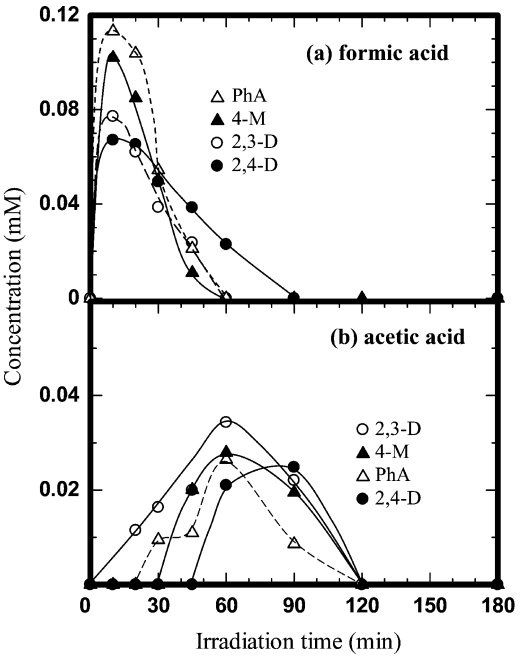

Fig. 4 Temporal formation of formic acid (a) and acetic acid (b) in the photodegradation of 2,4-D, 2,3-D, 4-M and PhA.

Identification of some of the more complex intermediates was achieved using LC-MSD electrospray ionization methods; mass spectra were recorded at various irradiation times from 0 to 180 min in the negative ion mode. Fig. 5 (left column) illustrates the relevant spectra at 0, 30, 60 and 180 min for the 2,4-D substrate, whereas the right column depicts those for the 2,3-D system after the same irradiation times. The signals at m/z 219, 221, and 223 in the mass spectrum of the initial solution correspond to the parent phenoxyacetic acid containing two chlorine substituents, while the three signals at 161, 163 and 165 are those of the corresponding dichlorophenol present in the solution either as an initial impurity, or produced from the workup of the solution in the electrospray mass spectral detector. Note that the spectra are presented relative to the most intense peak set at 100%. The spectra tend to be very complex with a multitude of peaks. It is noteworthy that the spectra for 2,4-D are difrerent from those of 2,3-D for equal irradiation times. This points to different routes for the degradation of the two systems. Not all the signals were identified as to their parentage. Those that were identified are described below and we present possible mechanistic route(s) of the fate of the various species.

Scheme 2 summarizes some of the hypothesized steps in the photodegradation of the 2,4-D substrate. From the results we infer two significant initial steps (**I**) and (**II**), which bring the 2,4-D to yield 2,4-dichlorophenol through cleavage of the O-*7*–C-*8* bond or through addition of the •OH radical at the C-*1* carbon bearing the highest electron density in the 2,4-D substrate (Table 1), and 6-hydroxy-2,4-dichlorophenoxyacetic acid on addition of an OH group at the C-*6* carbon. Partial dechlorination of the dichlorophenol occurs by •OH radical attack on the C-*4* carbon, which also bears the highest electron density, to give the corresponding chlorohydroquinone (m/z at 143 and 145, consistent with one chlorine substituent). Further reaction causes loss of the chlorine and cleavage of the ring to yield the intermediates with molecular weight of 130 and 113

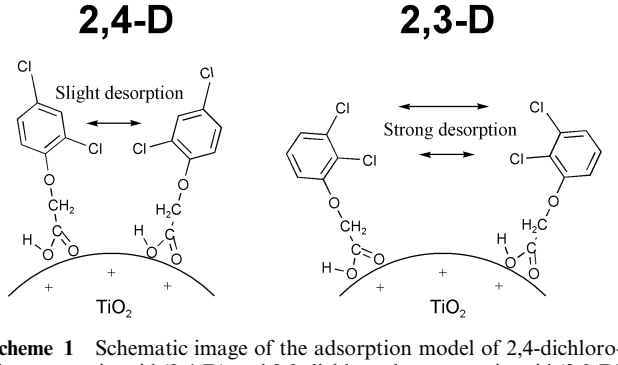

Scheme 1 Schematic image of the adsorption model of 2,4-dichlorophenoxyacetic acid (2,4-D) and 2,3-dichlorophenoxyacetic acid (2,3-D) on the TiO_2 surface.

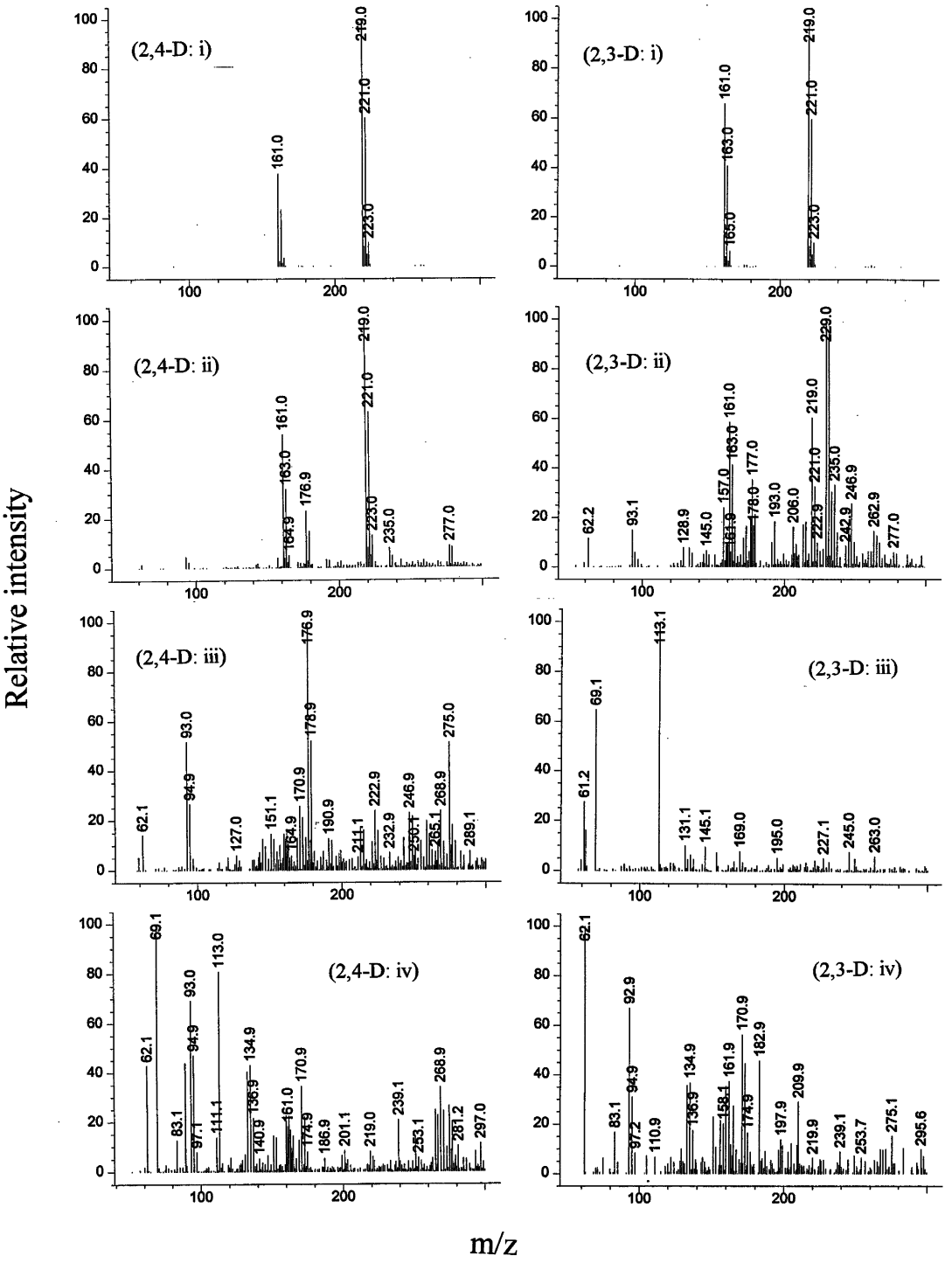

Fig. 5 Negative ion ESI mass spectra (i–iv) recorded in the photodecomposition of 2,4-D (left column) and 2,3-D (right column) at 0, 30, 60 and 180 min of UV illumination of the corresponding TiO_2 dispersions.

(negative ion peaks at $m/z = 129$ and 112), respectively. The 3,5-dichloro-1,2-benzenediol intermediate (MW = 179; m/z at 177, 179 and 181) is produced either from the dichlorophenol or from the intermediate (route **II**) with molecular weight 237 (m/z peaks at 235, 237, 239). The rapid formation of formic acid [in *ca.* 10 min of irradiation; see Fig. 4(a)] originates from the –COOH fragment of 2,4-D (see above), which should have produced either the dichlorophenoxymethanol species or dichlorophenoxymethane. Signals for the former are barely perceptible relative to the more intense peaks {see the 30 min and 60 min spectra in Fig. 5; route **III**}. Other intermediates are displayed in Scheme 2 and ultimately they too are photodegraded to carbon dioxide.

Some of the identified intermediates produced in the photodegradation of the 2,3-D substrate (m/z peaks at 219, 221 and 223; see Fig. 5, right column) and inferred mechanistic steps are illustrated and summarized in Scheme 3. From the results we deduce the existence of three possible routes for the photodegradation process. In the first (**I**), $^{\bullet}OH$ radical attack at the C-*1* carbon yields the related 2,3-dichlorophenol ($m/z = 161$, 163, 165) with formation of formic acid and then more slowly also acetic acid [see Fig. 4(b)]. The phenolic intermediate

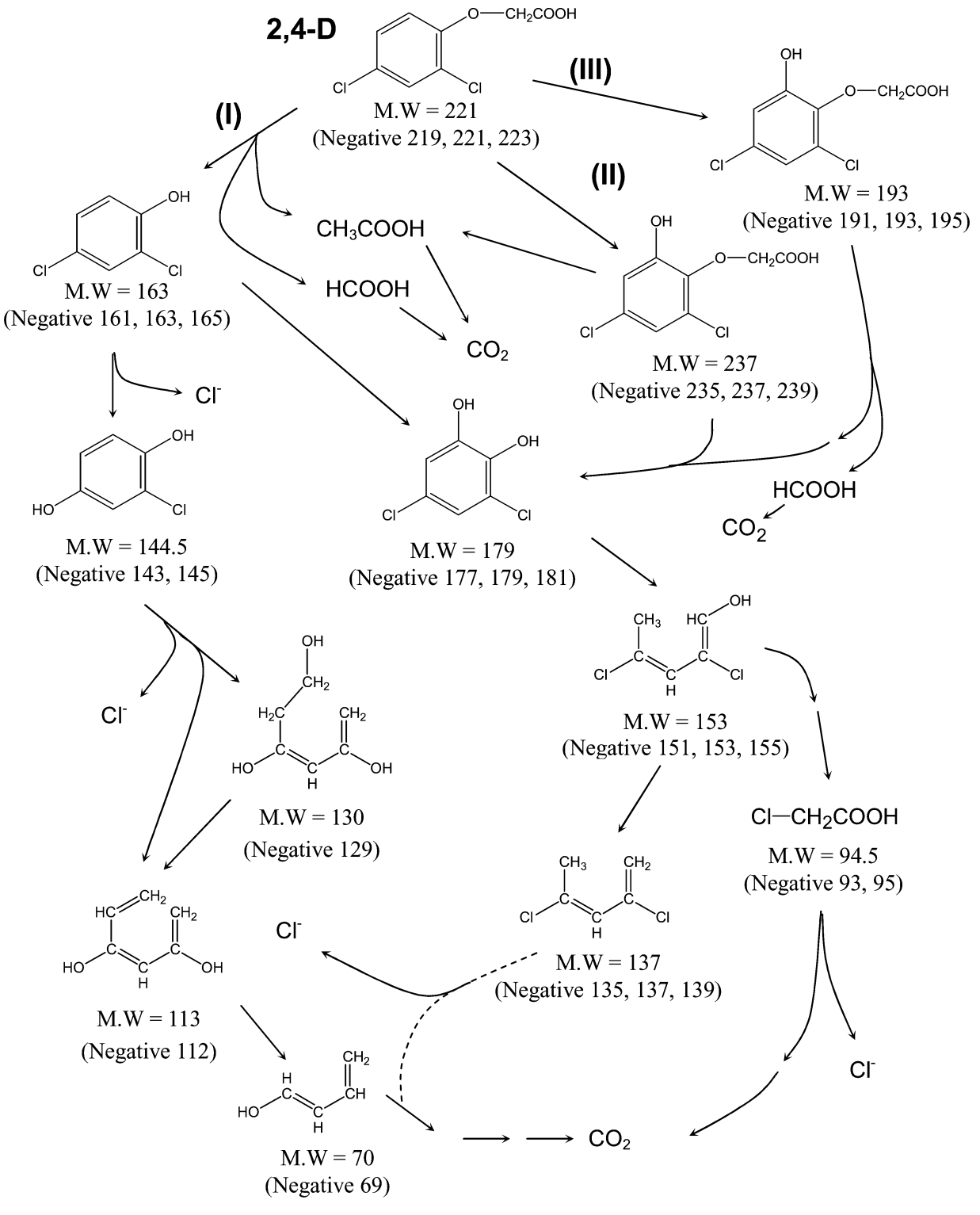

Scheme 2 Proposed photodegradation mechanism of 2,4-dichlorophenoxyacetic acid (2,4-D) under UV illumination in aqueous TiO_2 dispersions following identification of some of the intermediates by ESI mass spectral techniques.

subsequently undergoes further changes on attack at the C-*2* carbon (highest electron density for 2,3-D and, likely also, for this phenol) to produce the chlorocatechol species (m/z signals at 143 and 145) followed by another event to give the species with a peak in the negative ion mode spectra at m/z 129. In route **II**, as also seen for 2,4-D, the 6-hydroxy-2,3-dichlorophenoxyacetic acid intermediate forms (m/z at 235, 237, 239), followed by cleavage of the benzene ring to yield chloroacetic acid (m/z at 93, 95) and the chlorinated intermediate that appears at m/z = 177 and 179. The intermediate with m/z 95 and 97 is believed to be formed from the latter species. In route **III**, the parent substrate undergoes complete dechlorination (note that it is not unlikely that such a process also occur *via* a photoreductive process by electron attachment to 2,3-D) to yield the intermediate that appears at m/z 157, which is then followed by further degradative events to ultimately yield carbon dioxide.

Conclusions

This work has attempted to identify some of the salient mechanistic features in the photodegradation of the herbicide

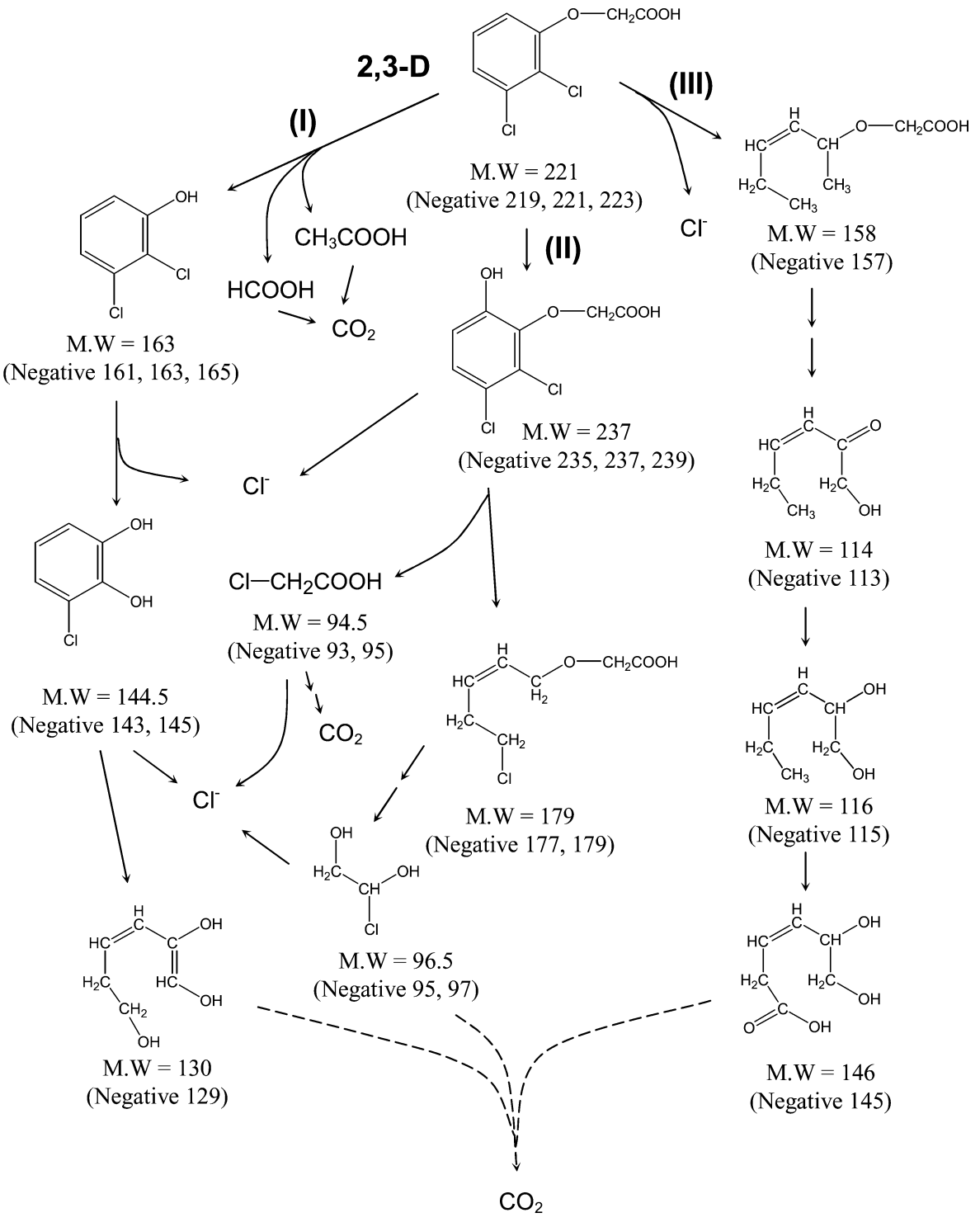

Scheme 3 Proposed photodegradation mechanism of 2,3-dichlorophenoxyacetic acid (2,3-D) under UV illumination in aqueous TiO_2 dispersions following identification of some of the intermediates by ESI mass spectral techniques.

2,4-D, extensively used in agriculture and which is causing some serious concerns for human health. Under the experimental conditions used in this study, the phenoxyacetic acids degraded fairly rapidly with about 80% mineralization and dechlorination achieved in about 2 h of UV irradiation. Electrospray ionization (ESI) mass spectral methods provided the necessary identification of some of the intermediates from rather complex mass spectra in which many of the intermediates remain yet to be identified. This notwithstanding, however, it is significant that substantial degradation of the herbicide is accomplished in a relatively short time from simple UV radiation, a degradative process that can also be driven by solar UV radiation.

Acknowledgements

We are grateful to the Frontier Research Promotion Foundation sponsored by the Japan Ministry of Education, Sports, Culture, Science and Technology (to H.H.) and to the Natural Sciences and Engineering Research Council of Canada (to N.S.) for support of our work.

References

1 E. Chamarro and S. Esplugas, *J. Chem. Technol. Biotechnol.*, 1993, **57**, 273.

2 P. Pichat, J. C. D'Oliveira, J. F. Maffre and D. Mas, in *Photocatalytic Purification and Treatment of Water and Air*, eds. D. F. Ollis and H. Al-Ekabi, Elsevier, Amsterdam, 1993, p. 683.
3 T. S. Muller, Z. Sun, G. Kumer M. P., K. Itoh and M. Murabayashi, *Chemosphere*, 1998, **36**, 2043.
4 A. D. Modestov and O. Lev, *J. Photochem. Photobiol., A*, 1998, **112**, 261.
5 T. Naguyen and D. F. Ollis, *J. Phys. Chem.*, 1984, **88**, 3386.
6 D. W. Bahnemann, J. Moning and R. Chapman, *J. Phys. Chem.*, 1987, **91**, 3782.
7 M. Barbeni, M. Morello, E. Pramauro, E. Pelizzetti, M. Vincenti, E. Borgarello, N. Serpone and M. A. Jamieson, *Chemosphere*, 1987, **16**, 1165.
8 F. Sabin, T. Turk and A. Vogler, *J. Photochem. Photobiol., A*, 1992, **63**, 99.
9 R. Borello, C. Minero, E. Pramauro, E. Pelizzetti, N. Serpone and H. Hidaka, *Environ. Toxicol. Chem.*, 1989, **8**, 997.
10 S. Horikoshi, N. Serpone, S. Yoshizawa, J. Knowland and H. Hidaka, *J. Photochem. Photobiol., A*, 1998, **120**, 63.
11 S. D. Kahn, C. F. Pau, L. E. Overman and W. J. Hehre, *J. Am. Chem. Soc.*, 1986, **108**, 7381.
12 H. Kaczmarek, A. Kamińska, M. Świątek and J. F. Rabek, *Angew. Makromol. Chem.*, 1998, **261**, 109.